Presented at the 35th European PV Solar Energy Conference and Exhibition, 24-28 September 2018, Brussels, Belgium

LASER-DOPED SELECTIVE EMITTER - PROCESS DEVELOPMENT AND SPEED-UP

J. Weber, S. Gutscher, S. Lohmüller, E. Lohmüller, A. A. Brand
Fraunhofer Institute for Solar Energy Systems ISE, Heidenhofstr. 2, 79110 Freiburg, Germany
Phone: +49 761 - 4588 5057; e-mail: julian.weber@ise.fraunhofer.de

ABSTRACT: This study pursues the development of a laser-doped selective emitter (LDSE) for p-type silicon passivated emitter and rear solar cells with screen-printed and fired silver contacts on the front. The LDSE is formed via local laser doping from the two-layer stack system of phosphosilicate glass and silicon dioxide that is located on the wafer surface after tube furnace diffusion using phosphorus oxychloride ($POCl_3$) as liquid dopant precursor. We aim for minimum emitter dark saturation current density at the LDSE-metal interface $j_{0e,met}$ and minimum specific contact resistance ρ_c. We use both an atmospheric pressure $POCl_3$ diffusion process and a high throughput low pressure $POCl_3$ diffusion process. Both $POCl_3$ processes are combined with a green nanosecond laser process at wavelength $\lambda = 532$ nm and pulse repetition rates 60 kHz $\leq f_{rep} \leq$ 100 kHz. Furthermore, we investigate high-speed infrared laser processes at $\lambda = 1064$ nm and $f_{rep} = 2$ MHz for which heat accumulation is expected to become relevant during LDSE formation. For some of the tested laser processes within this work, $\rho_c \approx 1$ mΩcm^2 is achieved. At the same time, simulations with the Quokka3 skin solver that are based on the LDSE doping profiles show that the LDSEs have the potential to lead to a $j_{0e,met}$ reduction by more than 50% compared to the not laser-doped emitter.
Keywords: Silicon Solar Cell, PERC, p-type, Selective Emitter, Laser Processing, Doping

1 INTRODUCTION

Within the field of passivated emitter and rear solar cell (PERC) technology, selective emitter concepts are again of great interest [1-4]. Gains of more than 0.3%$_{abs}$ in energy conversion efficiency are expected compared to the homogeneous emitter approach [2-5]. However, such a boost in energy conversion efficiency can only be realized, if both emitter dark saturation current density for the passivated emitter regions $j_{0e,pass}$ as well as for the metallized emitter regions $j_{0e,met}$ are reduced [5,6]. A decrease of $j_{0e,pass}$ can be achieved by reducing the surface doping concentration of the emitter within the photoactive area [6], whereas $j_{0e,met}$ can be reduced by heavily doping the emitter underneath the front metallization [4,7]. The heavily doped emitter should further allow for optimal electrical contact properties to allow for high fill factors and thus feature minimal specific contact resistance ρ_c. For p-type silicon solar cells, the most dominant technology for implementing a selective emitter [7] is local laser doping [8,9].

Within this study, laser-doped selective emitter (LDSE) processes are developed for p-type silicon PERC solar cells with screen-printed and fired silver contacts on the front. We aim for low $j_{0e,met} < 500$ fA/cm^2 and low $\rho_c < 2$ mΩcm^2. The LDSE is formed via local laser doping from a two-layer stack system consisting of phosphosilicate glass (PSG) and silicon dioxide (SiO_2). This layer stack system is located on the wafer surface after tube furnace diffusion using phosphorus oxychloride ($POCl_3$) as liquid dopant precursor. Thus, the interaction between the $POCl_3$ diffusion and the laser doping process is essential for the LDSE formation. In this work, three different process combinations are tested:

(i) We combine an atmospheric pressure (AP) $POCl_3$ diffusion process [3] and a green nanosecond laser process at wavelength $\lambda = 532$ nm and pulse repetition rate 60 kHz $\leq f_{rep} \leq$ 100 kHz (see section 4.1).

(ii) We switch from AP to low pressure (LP) $POCl_3$ diffusion [10-12] (see section 4.2). Within a LP system, the amount of processed wafers per cycle can be doubled, whereas the $POCl_3$ consumption is reduced [10]. Therefore, this technology is expected to play a major role in solar cell fabrication in the near future. In the long term, we thus aim for combining LDSE processes with a LP $POCl_3$ diffusion process.

(iii) We use the AP $POCl_3$ diffusion process from (i) for testing high-speed infrared (IR) laser doping processes at $\lambda = 1064$ nm and $f_{rep} = 2$ MHz (see section 5). When applying spatially overlapping laser pulses with such high repetition rates, consecutive laser pulses most likely interact with each other [13]. Heat is accumulated at the silicon surface which results in a drastic decrease of the absorption length, especially for IR laser irradiation [14]. The influence of this phenomenon on the LDSE formation has not yet been investigated. However, IR lasers are the most economical laser beam sources in terms of investment and operation. The approach (iii) allows for further speeding-up the LDSE formation, in order to achieve process times of clearly below one second per wafer. In this sense, the experiments performed at $f_{rep} = 2$ MHz not only address a new field of research, but are also relevant with regard to future LDSE developments.

2 APPROACH

For investigating LDSE processes, we use p-type Czochralski-grown silicon (Cz-Si) wafers with 156 mm edge length and an alkaline textured surface and apply the already mentioned different $POCl_3$ diffusion processes that are specially designed for the LDSE approach [3,12]. Laser test fields with an area of a few cm^2 are created consisting of overlapping laser lines. We vary laser process parameters, in particular laser pulse energy, pulse overlap, and pulse duration. Subsequent to laser doping, the wafers obtain a wet-chemical removal of the PSG layer and the emitter sheet resistance R_{sh} is determined via four-point-probe (4pp) measurements.

For a selection of test fields, charge carrier concentration profiles are recorded by electrochemical capacitance-voltage (ECV) measurements. Based on the 4pp measurements, the profiles are corrected as described in section 3. The corrected profiles are then used as input for the Quokka3 skin solver [15]. By setting the fundamental surface recombination velocity of electrons and holes to $S_n = S_p = 1 \cdot 10^7$ cm/s, we obtain an estimation for $j_{0e,met}$ [4]. However, $j_{0e,met}$ tends to be underestimated, since the formation of metal crystallites

between the silver contacts and the silicon surface as well as potentially increased recombination due to residual laser damage are neglected.

On some of the wafers, a silicon nitride (SiN_x) passivation layer is deposited and metal contacts with a width of about 40 µm are applied by screen-printing a commercially available silver paste. Subsequently, contact firing is performed at different set peak temperatures. To determine ρ_c, transmission line measurements (TLM) [16] are performed.

3 CORRECTION OF ECV PROFILES

ECV profiling enables recording the charge carrier concentration $N(z)$ within a doped semiconductor as a function of depth z. An excellent review on this technique is given in Ref. [17].

Fig. 1 shows three exemplary ECV measurements of identically processed laser test fields. One of the samples received a wet-chemical PSG removal, whereas for two of the samples, a PSG removal and an additional wet-chemical emitter etch back (EEB) are performed. Shifting the ECV profiles against each other shows good agreement between all measurements. However, a decrease of N towards the silicon surface is observed. This pile-down effect leads to a mismatch of the profiles and is thus interpreted as an artefact introduced by the ECV technique. The same conclusion was drawn by Kimmerle [18] when analyzing ECV measurements of not laser-processed samples. Also, in theory, rather a pile-up is expected for phosphorous-doped silicon, whereas a pile-down cannot be explained physically [19]. In consequence, for all of the ECV measurements within this work, the pile-down artefact is removed and the profiles are straightened in the surface-near region. In addition, the part of the profiles in which $N(z)$ is flattened by the influence of the base doping is cut off. In Fig. 1 this would be $N(z > 650$ nm). However, correction is not yet completed.

A further correction step is necessary, since during the ECV measurement, it is assumed that the surface area of the electrolyte-semiconductor interface, denoted by A, is plane. This assumption is false, since the textured and laser processed silicon surface exhibits a rough topography. The enlargement of the surface can be accounted for by introducing the factor f in the sense of $A^{corr} = fA$ [18]. The factor f can be found by adjusting the emitter sheet resistance resulting from the ECV profile to the 4pp measured sheet resistance [18,20]. This adjustment eventually yields the corrected doping profile [18]. For the doping profiles corrected within this work, $1.0 \leq f \leq 1.5$ is found.

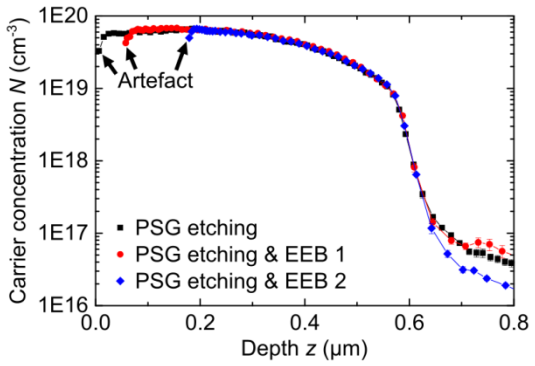

Figure 1: Exemplary ECV measured doping profiles of identically processed laser test fields showing a measurement artefact. All of the samples received a PSG removal. For two of the samples, an additional emitter etch back (EEB) is performed. The corresponding profiles are shifted to the right, so that they show the best possible match to the black squares.

4 PROCESS DEVELOPMENT

4.1 AP $POCl_3$ diffusion & green laser at $f_{rep} \leq 100$ kHz

For the first group of wafers, we apply an AP $POCl_3$ diffusion process that is specially designed for the LDSE approach [3]. The resulting emitter yields $j_{0e,pass} \approx 40$ fA/cm^2 for textured and SiN_x-passivated surfaces [3]. For creating the laser test fields, a nanosecond laser is used at $\lambda = 532$ nm and 60 kHz $\leq f_{rep} \leq$ 100 kHz. The $1/e^2$-radius of the laser beam is $\omega_0 = (50.0 \pm 0.4)$ µm. The position of the test fields is varied for each wafer, in order to account for inhomogeneities of the PSG layer across the wafers. In total, eight different parameter sets are tested differing in laser pulse energy E_p, (full width half maximum) pulse duration τ_p, and pulse pitch d_p (distance of the laser pulses within the laser lines as well as from line to line). For fabricating the TLM samples, two different set peak firing temperatures are chosen: 840 °C and 880 °C.

Fig. 2 shows R_{sh} and ρ_c in dependence on E_p, τ_p, d_p, and the set peak firing temperature, whereas the errors for E_p and τ_p are about 3%. We compare the laser-doped test fields with the emitter that results from AP $POCl_3$ diffusion and therefore serves as reference ("Ref"). Concerning the emitter sheet resistance, a drop from $R_{sh} \approx 140$ Ω/sq to 21 Ω/sq < R_{sh} < 49 Ω/sq after laser doping is observed. However, with increasing pulse duration τ_p, higher pulse energies E_p are necessary to achieve the same reduction in sheet resistance R_{sh}. In general, E_p shows a strong impact on R_{sh}. For the specific contact resistance ρ_c, an optimum occurs within the tested

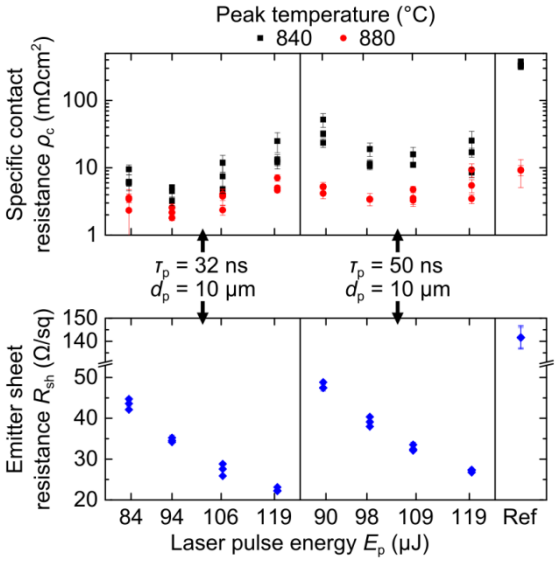

Figure 2: Emitter sheet resistance R_{sh} and specific contact resistance ρ_c as a function of laser pulse energy E_p and pulse duration τ_p for constant pulse pitch $d_p = 10$ µm. The emitter resulting from the AP $POCl_3$ diffusion process serves as reference ("Ref"). For ρ_c, a variation of the set peak firing temperature is shown.

range of E_p for both pulse durations. By increasing the set peak firing temperature from 840 °C to 880 °C, a decrease of ρ_c is obtained. For the shorter pulse duration τ_p = 32 ns, ρ_c tends to be lower than for the longer pulse duration τ_p = 50 ns. Minimal specific contact resistance $\rho_c \approx 2$ mΩcm^2 is achieved by τ_p = 32 ns, E_p = 94 µJ and 880 °C set peak firing temperature. For this temperature, the reference yields $\rho_c \approx 9$ mΩcm^2.

For some of the laser parameter sets shown in Fig. 2, ECV profiles are recorded. Again, the emitter that results from AP $POCl_3$ diffusion serves as reference. Fig. 3 sums up the corrected doping profiles, the factor f that is used for correction, and the corresponding Quokka3 estimations for $j_{0e,met}$. The laser-doped emitters are about 0.7 µm deep, which is about twice as deep as the reference emitter. Doping depth grows with increasing laser pulse energy E_p and pulse duration τ_p. For the reference emitter, we find the surface-near doping concentration $N_{surf} \approx 4 \cdot 10^{19}$ cm^{-3}. Laser doping does not change N_{surf} drastically. However, for the longer pulse duration τ_p = 50 ns, N_{surf} tends to be slightly reduced. Interestingly, both doping profiles obtained for the shorter pulse duration τ_p = 32 ns show an increase with growing depth z for z < 0.2 µm, which is unexpected from a physical point of view. The reason for this unexpected finding is not clear yet. Possibly, the observed increase is an artefact of the ECV measurement similar to the pile-down artefact (see Fig. 1) described in section 3. It is also possible that laser doping results in a local inhomogeneous charge carrier concentration. Such inhomogenities cannot be resolved by the ECV method, since the carrier concentration is averaged over several mm^2. The factor f that quantifies the enlargement of the surface is found to be f = 1.34 for the reference. By laser-doping, f is reduced. This can be explained by the fact that the surface gets molten and therefore smoothened during the laser process [8]. For τ_p = 32 ns, a decrease from f = 1.14 to f = 1.09 is found for increasing pulse energy from E_p = 94 µJ to E_p = 106 µJ. This is due to the increase in time in which the surface is molten [8]. The same effect is observed for τ_p = 50 ns. Here a reduction from f = 1.22 (E_p = 98 µJ) to f = 1.17 (E_p = 109 µJ) is obtained. Concerning the estimated $j_{0e,met}$, the amount of electrically active phosphorous atoms per area, which we call the phosphorous dose D, plays the major role [4]. If doping depth and surface-near doping concentration are increased, the phosphorous dose D grows and $j_{0e,met}$ is reduced. However, no drastic differences between the tested laser processes occur, since the phosphorous dose is within the same range of $D \approx 2 \cdot 10^{15}$ cm^{-2}. Compared to the reference ($D = 4 \cdot 10^{14}$ cm^{-2}), a reduction from $j_{0e,met}$ = 932 fA/cm^2 to 230 fA/cm^2 ≤ $j_{0e,met}$ ≤ 292 fA/cm^2 is achieved according to our estimation.

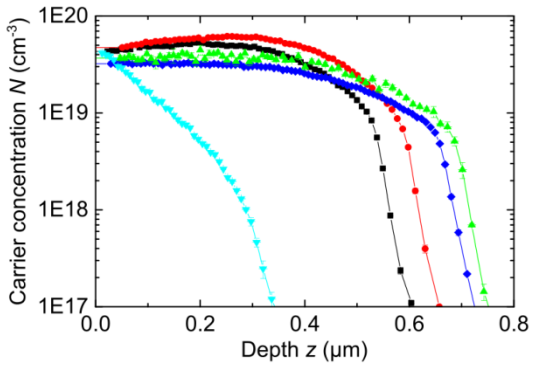

	E_p (µJ)	d_p (µm)	τ_p (ns)	f	$j_{0e,met}$ (fA/cm^2)
■	94	10	32	1.14	271
●	106	10	32	1.09	230
◆	98	10	50	1.22	292
▲	109	10	50	1.17	257
▼	Ref			1.34	932

Figure 3: Emitter doping profiles measured by ECV and corrected as discussed for some of the laser parameter sets shown in Fig. 2. The emitter resulting from the AP $POCl_3$ diffusion process serves as reference ("Ref"). For the correction, the factor f is used. Via Quokka3, the dark saturation current density at the emitter-metal interface $j_{0e,met}$ is estimated for each profile.

4.2 LP $POCl_3$ diffusion & green laser at $f_{rep} \leq 100$ kHz

For the second group of wafers, we use the same laser for creating the LDSE test fields as for the first wafer group. We stick to the short pulse duration τ_p = 32 ns and vary the pulse pitch d_p instead. Furthermore, we replace the AP $POCl_3$ diffusion process by a LP $POCl_3$ diffusion process. This LP process is similar to the one introduced in Ref. [12]. It is specially designed for the LDSE approach and yields $j_{0e,pass} \approx 43$ fA/cm^2 for textured and SiN_x-passivated surfaces. For fabricating the TLM samples, two different set peak firing temperatures are chosen: 810 °C and 850 °C.

Fig. 4 shows the results obtained for R_{sh} and ρ_c. We find that laser doping results in a reduction from $R_{sh} \approx 150$ Ω/sq to 36 Ω/sq < R_{sh} < 81 Ω/sq. The pulse energy E_p shows a strong impact on R_{sh}, whereas the pulse pitch d_p plays only a minor role. Interestingly, at E_p = 85 µJ, a decrease in R_{sh} is obtained for increasing the pitch from d_p = 10 µm to d_p = 25 µm, even though the applied energy per area is reduced. This counterintuitive finding could be due to variations within the properties of the PSG/SiO_2 layer system and the reference emitter that are caused by inhomogenities within the $POCl_3$ diffusion

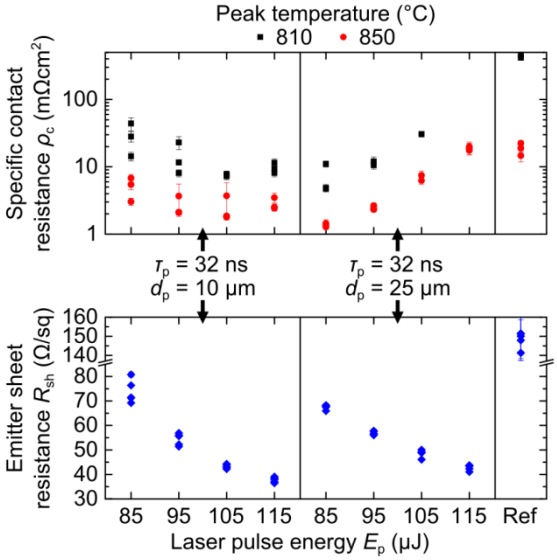

Figure 4: Emitter sheet resistance R_{sh} and specific contact resistance ρ_c as a function of laser pulse energy E_p and pulse pitch d_p for constant pulse duration τ_p = 32 ns. The emitter resulting from the LP $POCl_3$ diffusion process serves as reference ("Ref"). For ρ_c, a variation of the set peak firing temperature is shown.

process. Concerning ρ_c, an optimum is found for d_p = 10 µm. This is in good accordance with the corresponding results obtained for the AP $POCl_3$ diffusion process (τ_p = 32 ns and d_p = 10 µm in Fig. 2). For both AP and LP $POCl_3$ diffusion process, minimal specific contact resistance $\rho_c \approx 2$ mΩcm^2 is reached for $E_p \approx 100$ µJ. For the LP $POCl_3$ diffusion process and d_p = 25 µm (see Fig. 4), we expect the minimum of ρ_c to be reached at $E_p < 85$ µJ. However, within the tested pulse energy range, 1 mΩcm^2 < ρ_c < 2 mΩcm^2 is achieved at 850 °C, whereas the reference yields $\rho_c \approx 19$ mΩcm^2. For 810 °C, ρ_c is found to increase.

For a selection of test fields, doping profiles are recorded and $j_{0e,met}$ is estimated. Fig. 5 sums up the results. If pulse energy is raised, the doping depth increases. Compared to the reference, profile depth is enlarged from about 0.3 µm to about 0.5 µm (E_p = 85 µJ) and 0.7 µm (E_p = 115 µJ), respectively. By changing the pulse pitch from d_p = 10 µm to d_p = 25 µm, the doping profiles are steepened and surface-near doping concentration is increased by more than $\Delta N_{surf} \approx 1 \cdot 10^{19}$ cm^{-3}. For E_p = 85 µJ, this increase yields $N_{surf} \approx 4 \cdot 10^{19}$ cm^{-3}, whereas for E_p = 115 µJ, $N_{surf} \approx 5 \cdot 10^{19}$ cm^{-3} is obtained. For the factor f that is used to correct the doping profiles, similar trends as in section 4.1 are observed. The reference yields f = 1.50, which is the largest value that is found. By laser-doping, f is reduced. This reduction strongly depends on the laser pulse energy E_p, whereas the pulse pitch plays only a minor role. For E_p = 85 µJ, $f \approx 1.32$ is found, whereas E_p = 115 µJ yields $f \approx 1.05$.

Concerning the $j_{0e,met}$ estimation, significant differences for the laser-doped test fields are obtained which reflects the differences in doping dose [4]. By all tested LDSE processes, however, a drastic reduction from $j_{0e,met}$ = 1070 fA/cm^2 to $j_{0e,met} \leq 489$ fA/cm^2 is achieved according to the estimation. For d_p = 25 µm, a tradeoff between $j_{0e,met}$ and ρ_c exists within the tested range of E_p, since ρ_c but also the doping dose decreases when laser pulse energy is reduced.

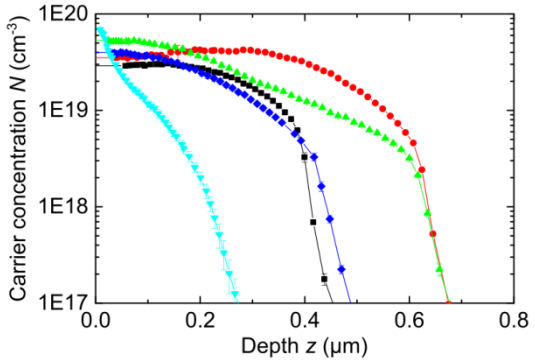

	E_p (µJ)	d_p (µm)	τ_p (ns)	f	$j_{0e,met}$ (fA/cm^2)
■	85	10	32	1.35	489
●	115	10	32	1.08	281
◆	85	25	32	1.29	469
▲	115	25	32	1.02	313
▼	Ref			1.50	1070

Figure 5: Emitter doping profiles measured by ECV and corrected as discussed for some of the laser parameter sets shown in Fig. 4. The emitter resulting from the LP $POCl_3$ diffusion process serves as reference ("Ref"). For the correction, the factor f is used. Via Quokka3, the dark saturation current density at the emitter-metal interface $j_{0e,met}$ is estimated for each profile.

Comparing the results of this section with the ones obtained for the AP $POCl_3$ diffusion process presented in section 4.1, we identify the most promising approach to be the combination of the LP $POCl_3$ diffusion process with the LDSE process at τ_p = 32 ns, E_p = 85 µJ, and d_p = 25 µm. By this approach, the throughput of the $POCl_3$ diffusion process is increased and minimal specific contact resistance $\rho_c \approx 1$ mΩcm^2 is achieved. However, an experimental analysis of $j_{0e,pass}$ and $j_{0e,met}$ for the tested LDSE processes is required for a more sophisticated process development.

5 PROCESS SPEED-UP

For the third group of wafers, we apply the same AP $POCl_3$ process as for the first group. Laser doping, however, is performed using an IR laser (λ = 1064 nm) at constant repetition rate f_{rep} = 2 MHz, pulse duration $\tau_p \approx 30$ ns, and 1/e^2-radius $\omega_0 \approx 28$ µm. A polygon scanner system [22] is used to create laser lines with scan speeds $v_s \geq 40$ m/s and a constant line pitch of 10 µm. For these laser parameters, we expect heat accumulation [13] to occur during the LDSE formation.

Within a first experiment, we test two laser processes *A* and *B* differing only in scan speed v_s. As Fig. 6 shows, after applying laser process *A*, no modification of the wafer surface is observed. In contrast, for process *B* for which the spatial overlap of the laser pulses within each laser line is increased, the threshold of modification is exceeded. This could be due to an enhanced heat accumulation resulting from the increase in overlap of the pulses. However, these observations can only be interpreted as an indication for the presence of heat accumulation.

We use process *B* as a starting point for testing potential high-speed laser processes for LDSE formation. In order to achieve significant doping, we raise pulse energy to E_p = 44 µJ and E_p = 47 µJ, respectively, while keeping the scan speed at v_s = 40 m/s. For both pulse energies, one test field is processed and characterized by 4pp and ECV. Fig. 7 summarizes the obtained results. Both doping profiles exhibit a surface-near doping concentration of $N_{surf} \approx 4 \cdot 10^{19}$ cm^{-3}. With increasing depth, the doping profiles start to differ from each other. For E_p = 44 µJ, the doping depth is below 1 µm. We obtain R_{sh} = 47 Ω/sq and $j_{0e,met}$ = 335 fA/cm^2. In contrast, E_p = 47 µJ yields a doping depth larger than 1 µm and thus a reduction in R_{sh} of about ΔR_{sh} = 8 Ω/sq and an

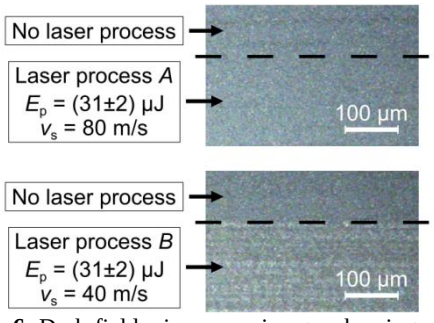

Figure 6: Dark-field microscope images showing parts of the wafer surface after performing the AP $POCl_3$ diffusion process and applying laser processes *A* and *B* with identical laser pulse energy E_p. A modification of the surface is observed by decreasing the scan speed v_s.

increase in $j_{0e,met}$ of $\Delta j_{0e,met}$ = 49 fA/cm^2. Concerning the factor f, we find a slight decrease from f = 1.10 to f = 1.05 for increasing laser pulse energy. As already mentioned, this can be explained by the increase in time in which the wafer surface is molten during laser doping.

Compared to the doping profiles shown in Fig. 3 and Fig. 5, the high-speed laser processes yield steeper emitter profile and an increased doping depth. However, in terms of R_{sh}, f, estimated $j_{0e,met}$, and N_{surf}, similar results are achieved. Nevertheless, further research is necessary to investigate, if also for high-speed IR laser processes, low specific contact resistance ρ_c < 2 mΩcm^2 can be achieved. Also, deeper knowledge is required concerning the phenomenon of the heat accumulation.

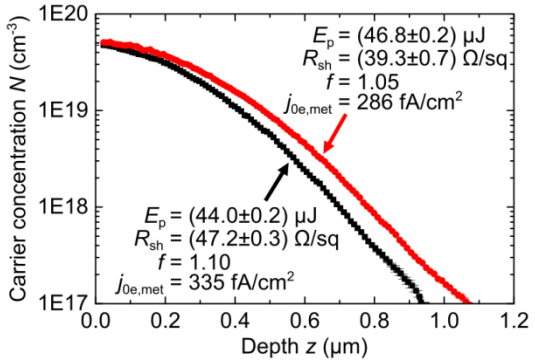

Figure 7: Emitter doping profiles measured by ECV and corrected by the factor f, emitter sheet resistance R_{sh}, and estimated dark saturation current density at the emitter-metal interface $j_{0e,met}$ for two laser processes with constant scan speed v_s = 40 m/s and differing laser pulse energy E_p. Laser doping is combined with the AP $POCl_3$ diffusion process.

6 SUMMARY AND CONCLUSION

Within this work, we develop laser-doped selective emitter (LDSE) processes for p-type silicon passivated emitter and rear solar cells with screen-printed and fired silver contacts on the front. For local laser doping, we use the two-layer stack system of phosphosilicate glass and silicon dioxide that is located on top of the silicon surface after phosphorus oxychloride ($POCl_3$) tube furnace diffusion. For the LDSE doping profiles that are recorded within this work, the emitter dark saturation current density at the LDSE-metal interface is reduced to 230 fA/cm^2 ≤ $j_{0e,met}$ ≤ 489 fA/cm^2, which is a reduction of more than 50% compared to the not laser-doped emitter according to a Quokka3 estimation. For the combination of the atmospheric pressure $POCl_3$ diffusion process and the green nanosecond laser at wavelength λ = 532 nm, specific contact resistance $\rho_c \approx 2$ mΩcm^2 is achieved by using laser pulse energy E_p = 94 µJ, pulse duration τ_p = 32 ns, and pulse pitch d_p = 10 µm. For the low pressure $POCl_3$ diffusion process with increased throughput, $\rho_c \approx 1$ mΩcm^2 is achieved by E_p = 85 µJ, τ_p = 32 ns, and d_p = 25 µm. When applying high-speed infrared (IR) laser processes at pulse repetition rate f_{rep} = 2 MHz, we expect heat accumulation to occur. However, further research is necessary to understand under which conditions this phenomenon becomes relevant and how it affects the doping profile of the LDSE, the crystal structure, and the properties of the LDSE-metal interface, in particular the specific contact resistance.

ACKNOWLEDGEMENTS

This work was funded by the German Federal Ministry for the Environment, Nature Conservation and Nuclear Safety within the research project “POLDI” (Contract Number 0324079D).

REFERENCES

[1] M. Müller. G. Fischer, B. Bitnar et al., "22.61% efficient fully screen printed PERC solar cell," Energy Procedia, vol. 124, pp. 131-137, 2017.

[2] S. Wasmer, A. A. Brand, and J. M. Greulich, "Metamodeling of numerical device simulations to rapidly create efficiency optimization roadmaps of monocrystalline silicon PERC cells," Energy Procedia, vol. 124, pp. 207-214, 2017.

[3] S. Werner, E. Lohmüller, P. Saint-Cast et al., "Key aspects for fabrication of p-type Cz-Si PERC solar cells exceeding 22% conversion efficiency," in 33rd European Photovoltaic Solar Energy Conference and Exhibition, 2017, pp. 406-412.

[4] J. Weber, S. Lohmüller, E. Lohmüller et al., "Simulations on laser-phosphorous-doped selective emitters," in 7th World Conference on Photovoltaic Energy Conversion, to be published, 2018.

[5] A. Wolf, A. Kimmerle, S. Werner et al., "Status and perspective of emitter formation by POCl3-diffusion," in 31st European Photovoltaic Solar Energy Conference and Exhibition, 2015, pp. 414-419.

[6] S. Werner, E. Lohmüller, S. Maier et al., "Challenges for lowly-doped phosphorus emitters in silicon solar cells with screen-printed silver contacts," Energy Procedia, vol. 124, pp. 936-946, 2017.

[7] ITRPV, "International technology roadmap for photovoltaic (ITRPV) - 2017 Results - Ninth edition, March 2018," available online: http://www.itrpv.net/Reports/Downloads/, 2018.

[8] U. Jäger, "Selektive Laserdiffusion für hocheffiziente Solarzellen aus kristallinem Silicium," München: Verlag Dr. Hut, 2013.

[9] L. Ventura, A. Slaoui, and J. C. Muller, "Realization of selective emitters by rapid thermal and laser assisted techniques," in 13th European Photovoltaic Solar Energy Conference and Exhibition, 1995, pp. 1578-1581.

[10] M. Mühlbauer, A. Piechulla, C. Voyer et al., "Industrial low-pressure phosphorus diffusion for high performance and excellent uniformity," in 26th European Photovoltaic Solar Energy Conference and Exhibition, 2011, pp. 2028-2030.

[11] S. Lohmüller, S. Schmidt, E. Lohmüller et al., "Transfer of $POCl_3$ diffusion processes from atmospheric pressure to high throughput low pressure," AIP Conference Proceedings, vol. 1999, pp. 070002-1-070002-6, 2018.

[12] S. Lohmüller, M. Meßmer, S. Schmidt et al., "Analysis of phosphosilicate glass structures formed by atmospheric pressure and high throughput low pressure $POCl_3$ diffusion," in 7th World Conference

on Photovoltaic Energy Conversion, to be published, 2018.
[13] R. Weber, T. Graf, P. Berger et al., "Heat accumulation during pulsed laser materials processing," Optics Express, vol. 22, pp. 11312-11324, 2014.
[14] E. H. Sin, C. K. Ong, and H. S. Tan, "Temperature dependence of interband optical absorption of silicon at 1152, 1064, 750, and 694 nm," Physica Status Solidi (a), vol. 85, pp. 199-204, 1984.
[15] A. Fell, J. Schön, M. C. Schubert et al., "The concept of skins for silicon solar cell modeling," Solar Energy Materials and Solar Cells, vol. 173, pp. 128-133, 2017.
[16] H. H. Berger, "Contact resistance and contact resistivity", Journal of the Electrochemical Society, vol. 119, pp. 507–514, 1972.
[17] P. Blood, "Capacitance-voltage profiling and the characterisation of III-V semiconductors using electrolyte barriers," Semiconductor Science and Technology, vol. 1, pp. 7-27, 1986.
[18] A. Kimmerle, "Diffused surfaces for crystalline silicon solar cells - process development, characterization, and modeling," PhD thesis, University of Freiburg, Germany, 2015.
[19] A. S. Grove, O. Leistiko, and C. T. Sah, "Redistribution of acceptor and donor impurities during thermal oxidation of silicon," Journal of Applied Physics, vol. 35, pp. 2695-2701, 1964.
[20] R. Bock, P. Altermatt, and J. Schmidt, "Accurate extraction of doping profiles from electrochemical capacitance voltage measurements," in 23rd European Photovoltaic Solar Energy Conference and Exhibition, 2008, pp. 1510-1513.
[21] D. B. M. Klaassen, "A unified mobility model for device simulation - I. model equations and concentration dependence," Solid-State Electronics, vol. 35, pp. 953-959, 1992.
[22] R. De Loor, "Polygon scanner system for ultra short pulsed laser micro-machining applications," Physics Procedia, vol. 41, pp. 544-551, 2013.